Physics implications of shape on biological function
Pomp, W.

Citation
Pomp, W. (2017, December 5). *Physics implications of shape on biological function. Casimir PhD Series*. Retrieved from https://hdl.handle.net/1887/57789

Cover Page

Author: Pomp, Wim
Title: Physics implications of shape on biological function
Date: 2017-12-05

Chapter 4

Cytoskeletal anisotropy controls geometry and forces of adherent cells[†]

We introduce a simple mechanical model for adherent cells that quantitatively relates cell shape, internal cell stresses and traction forces as generated by an anisotropic cytoskeleton. Using a combination of analytic work and experiments on micropillar arrays, we demonstrate that the shape of the cell edge is accurately described by elliptical arcs, whose eccentricity expresses the degree of anisotropy of the internal cell stresses. Our work highlights the strong interplay between cell mechanics and geometry and paves the way towards the reconstruction of cellular forces from geometrical data.

4.1   Introduction

Cell behavior and fate crucially depend on mechanical cues from outside the cell [1–5]. Examples include rigidity-dependent stem cell differentiation [6, 7], protein expression regulated by internal stresses [8], and durotaxis [9, 10]. Whether at rest on a substrate [11] or migrating [12, 13], cells rely on their shape to gauge the mechanical properties of their microenvironment [14] and control the traction force exerted on their surroundings. The physical mechanisms behind these spectacular forms of bio-mechanical adaptation are, however, poorly understood.

Many animal cells spread and develop transmembrane adhesion receptors when coming into contact with an adhesive substrate. This induces the actin cytoskeleton to reorganize into cross-linked networks and bundles (i.e. stress fibers), whereas adhesion becomes limited to a number of sites, distributed mainly along the cell contour (i.e. focal adhesions). At this stage, cells are essentially flat and assume a typical shape characterized by arcs which span between the sites of adhesion, while forces are mainly contractile [15]. On timescales much shorter than those required by a cell to change its shape (i.e. minutes), the cell is in mechanical equilibrium at any point of its interface.

4.2   Model

We model adherent cells as two-dimensional contractile films [16], and we focus on the shape of the cell edge connecting two consecutive adhesion sites. Mechanical equilibrium requires the difference between the internal and external stresses acting on the cell edge to balance the contractile forces arising in the cortex:

$$\frac{\mathrm{d}\boldsymbol{F_{\mathbf{cortex}}}}{\mathrm{d}s} + (\hat{\boldsymbol{\Sigma}}_{\mathrm{out}} - \hat{\boldsymbol{\Sigma}}_{\mathrm{in}}) \cdot \boldsymbol{N} = \boldsymbol{0} \; . \tag{4.1}$$

Here $\hat{\boldsymbol{\Sigma}}_{\mathrm{out}}$ and $\hat{\boldsymbol{\Sigma}}_{\mathrm{in}}$ are the stress tensors outside and inside the cell and $\boldsymbol{F}_{\mathrm{cortex}}$ is the stress resultant along the cell cortex. The latter is parametrized as a one-dimensional curve spanned by the arc-length s and oriented along the inward pointing normal vector $\boldsymbol{N}$. A successful approach, initially proposed by Bar-Ziv $et\ al.$ in the context of cell pearling [17] and later expanded by Bischofs $et\ al.$ [11, 18], consists of modelling bulk contractility in terms of an isotropic pressure $\hat{\boldsymbol{\Sigma}}_{\mathrm{out}} - \hat{\boldsymbol{\Sigma}}_{\mathrm{in}} = \sigma\hat{\boldsymbol{I}}$, with $\hat{\boldsymbol{I}}$ the identity matrix, and peripheral contractility as an interfacial tension of the form $\boldsymbol{F}_{\mathrm{cortex}} = \lambda\boldsymbol{T}$, with $\boldsymbol{T}$ a unit vector tangent to the cell edge. The quantities σ and λ are material constants that embody the biomechanical activity of myosin motors in the

actin cytoskeleton. This competition between bulk and peripheral contractility along the cell boundary results in the formation of arcs of constant curvature $1/R = \sigma/\lambda$, through a mechanism analogous to the Young-Laplace law for fluid interfaces. The shape of the cell boundary is then approximated by a sequence of circular arcs, whose radius R might or might not be uniform across the cell, depending on how the cortical tension λ varies from arc to arc. The case of shape-dependent λ values was elaborated by Bischofs *et al* [11, 18] to account for an apparent correlation between the curvature and length of the cellular arcs. Both models successfully describe the geometry of adherent cells in the presence of strictly isotropic forces.
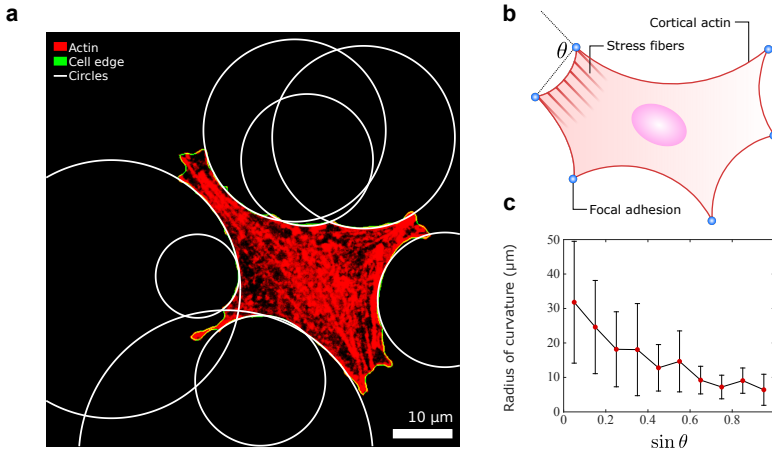

Figure 4.1: **Relation between stress fibres and curvature of the cell edge. a** A cell with an anisotropic actin cytoskeleton (epithelioid GEβ3) with circles (white) fitted to its edges (green). The actin cytoskeleton is visualised with TRITC-Phalloidin (red). Scalebar is 10 μm. **b** The cell cortex (red line) is spanned in segments between fixed adhesion sites (blue). The line through two adhesion sites makes an angle θ with the stress fibres inside the cell. **c** Arc radius as a function of $\sin\theta$ (data show the mean $\pm$ standard deviation).

4.3   The actin cytoskeleton is anisotropic

Yet many cells, including the fibroblastoids (GDβ1, GDβ3) and epithelioids (GEβ1, GEβ3) studied here (figure 4.1a) [19], develop directed forces by virtue of the strong anisotropic cytoskeleton originating from the actin stress fibers [20, 21]. This scenario is, evidently, beyond the scope of models based on isotropic contractility. Indeed, while the shape of the cell edges in Fig. 1a can still be approximated by circular arcs, the large variance in the distribution of R appears unjustified, as it would imply large variations in the cortical tension λ. Furthermore, a survey of a sample of 285 cells did not reveal a correlation between the length and the radius of the circular arcs, as predicted by the tension-elasticity model discussed by Bischofs *et al* [11, 18]. On the other hand, our data show a prominent correlation between the radius of curvature of the cellular arcs and their angle θ with respect to the local orientation of stress fibers (figure 4.1b). In particular, the radius of curvature decreases as the stress fibers become more perpendicular to the cell cortex (figure 4.1c). This correlation is intuitive as the bulk contractile stress focusses in the direction of the stress fibers.

The anisotropy of the actin cytoskeleton can be incorporated into the mechanical framework summarised by equation (4.1), by modelling the stress fibres as contractile force-dipoles. This collectively gives rise to a directed contractile bulk stress, namely $\hat{\mathbf{\Sigma}}_{\text{out}} - \hat{\mathbf{\Sigma}}_{\text{in}} = \sigma\hat{\boldsymbol{I}} + \alpha\boldsymbol{nn}$ [22, 23], with $\alpha > 0$ the magnitude of the directed contractile stress and $\boldsymbol{n}$ the average direction of the stress fibres. The ratio between isotropic contractility σ and directed contractility α measures the degree of anisotropy of the bulk stress. With this stress tensor the force balance equation (4.1) becomes:

$$\frac{\mathrm{d}\lambda}{\mathrm{d}s}\boldsymbol{T} + (\lambda\kappa + \sigma)\boldsymbol{N} + \alpha(\boldsymbol{n}\cdot\boldsymbol{N})\boldsymbol{n} = \boldsymbol{0} \, , \qquad (4.2)$$

where we used $\mathrm{d}\boldsymbol{T}/\mathrm{d}s = \kappa\boldsymbol{N}$, with κ the curvature of the cell edge. This implies that, in the presence of an anisotropic cytoskeleton, the cortical tension λ is no longer constant along the cell cortex, as long as the directed stress has a non-vanishing tangential component (i.e. $\boldsymbol{n}\cdot\boldsymbol{T} \neq 0$).

When the orientation of the stress fibres is approximately constant along a single cellular arc (figure 4.2a), a general solution of equation (4.2) is straightforwardly obtained. Taking without loss of generality $\boldsymbol{n} = \hat{\boldsymbol{y}}$, yields the shape of a cellular arc in implicit form:

$$\frac{\sigma^2}{\gamma\lambda_-^2}\,x^2 + \frac{\sigma^2}{\lambda_-^2}\,y^2 = 1 \, , \qquad (4.3)$$
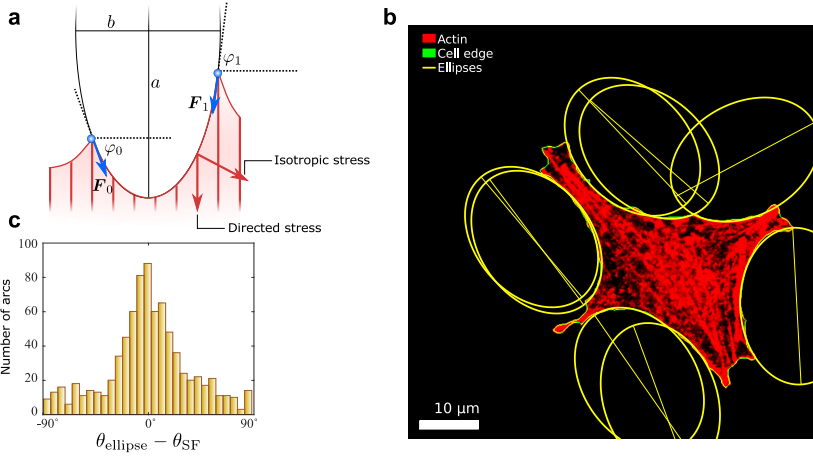
Figure 4.2: **The anisotropic cytoskeleton is reflected in the elliptical shape of the cell edge.** (a) Schematic representation of our model. A force balance between isotropic stress, directed stress and line tension results in the description of each cell edge segment (red curve) as part of an ellipse of aspect ratio $b/a = \sqrt{\gamma}$, unique to each cell. The cell exerts forces $\boldsymbol{F}_0$ and $\boldsymbol{F}_1$ on the adhesion sites (blue) with magnitude $\lambda(\varphi_0)$ and $\lambda(\varphi_1)$. (b) An epithelioid cell (same cell as in Fig. 1a) with a unique ellipse (yellow) fitted to its edges (green). The orientations of the major axes (yellow lines) are parallel to the local orientations of the stress fibers. Scalebar is 10 μm. (c) Histogram of $\theta_{\text{ellipse}} - \theta_{\text{SF}}$, with θ_{ellipse} the orientation of the fitted ellipse and θ_{SF} the measured orientation of the stress fibres. The mean of this distribution is 0° and the standard deviation is 36°.

where $\gamma = \sigma/(\sigma + \alpha)$ and λ_- is a constant that characterises the cortical tension and will be discussed in more detail later. Equation (4.3) describes an ellipse of aspect ratio $\sqrt{\gamma}$ and major semi-axis λ_-/σ, as illustrated in figure 4.2a. The dimensionless quantity γ highlights the interplay between the forces experienced by the cell edge and its shape: on the one hand, γ characterises the anisotropy of the bulk stress, while on the other hand it determines the anisotropy of the cell shape. Furthermore, as $0 \leq \gamma \leq 1$, it follows from equation (4.3) that the major axis of the ellipse is oriented parallel to the stress fibres (figure 4.2a).

The key prediction of our model is illustrated in figure 4.2b and in figure 4.4, where we have fitted the contour of the same cell shown in figure 4.1a with ellipses. Whereas large variations in the circles' radii were required in figure 4.1a, a unique ellipse ($\gamma = 0.52$, $\lambda_-/\sigma = 13.4\,\mu\mathrm{m}$) faithfully describes all the arcs in the cell. While fitting, the directions of the major axes were fixed to be parallel to the local orientations of the stress fibers. To test the accuracy of this latter choice, we fitted unconstrained and independent ellipses to all cellular arcs in our database. The distribution of the difference between the orientation $\theta_{\mathrm{ellipse}}$ of the fitted ellipse and the measured orientation θ_{SF} of the stress fibers is shown in Fig. 2c. The distribution peaks at $0°$ and has a width of $36°$, demonstrating that the orientation of the ellipses is parallel, on average, to the local orientation of the stress fibers as predicted by our model.
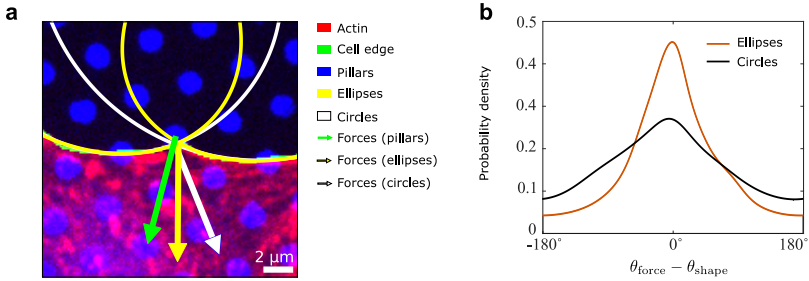

Figure 4.3: **Analysis of the shape of a cell allows to predict the orientations of traction forces.** **a** Zoom-in on one adhesion site of the cell in the previous figures. Actin is shown in red, the cell edge in green and the tops of the micropillars in blue. Additionally, the fitted ellipses (yellow) and circles (white) and the measured force (green) on the adhesion site, as well as the orientations of the forces calculated using the tension-elasticity model (white) [11], and the model presented in this chapter (yellow) are shown. Scalebar is 2 μm. **b** Histogram (shown as a probability density) of $\theta_{\mathrm{force}} - \theta_{\mathrm{shape}}$ for our anisotropic model (red) and the isotropic tension-elasticity model (black). Both the distributions are centered around $0°$, the standard deviations are $60°$ and $40°$ for the isotropic and anisotropic models respectively.

Equation (4.2) further allows to analytically calculate the cortical tension λ. Namely,

$$\lambda(\varphi) = \lambda_- \sqrt{\frac{1 + \tan^2(\varphi)}{1 + \gamma \tan^2(\varphi)}} \, , \tag{4.4}$$

where φ is the orientation of the tangent vector $\boldsymbol{T}$ with respect to an axis perpendicular to the stress fibres (Fig. 2a). The function λ attains its minimum value at the point along the cellular arc where $\varphi = 0$ and $\lambda(0) = \lambda_-$. Here, the cortical tension has no contribution from the directed stress (i.e. $\boldsymbol{n} \cdot \boldsymbol{T} = 0$), thus λ_- can be interpreted as the intrinsic tension along the cell cortex and, together with σ and α, represents a material parameter of our model.

Equation (4.3) and equation (4.4) are used to predict the traction force exerted by the cell at a specific adhesion site by adding the cortical tension $\lambda \boldsymbol{T}$ along the two cellular arcs joining at the adhesion site. We emphasize that this analysis yields information on cellular forces solely based on the analysis of cell shape. For example, the direction of the traction forces is calculated without additional fitting parameters. We compare the result with the direction of the traction force measured with a micropillar array technology [24–26]. An example is shown in figure 4.3a for one of the adhesion points of the cell in figure 4.2b, more examples are shown in figure 4.4 and figure 4.5. The arrows mark the direction of the measured traction force (green) and that calculated by approximating the cell shape with ellipses (yellow). As a comparison figure 4.3a also shows a prediction based on circles from the isotropic tension-elasticity model (white) [11, 18].

Data for all 285 cells are summarised in figure 4.3b, where we show the distribution of the orientation difference between the force direction predicted by our model θ_{shape} and its experimentally obtained value θ_{force}. Across the cell types used, the predicted distribution is centered at $0°$ and has a width of $40°$. As a comparison, we plot also the result for the earlier isotropic model which displays a significantly larger width of the distribution of $60°$. This significant improvement shows that not only cell shape, but also adhesion forces are profoundly affected by the anisotropy of the cytoskeleton.

γ	λ_- (nN)	σ (nN/µm)	α (nN/µm)
0.33 ± 0.20	7.6 ± 5.6	0.87 ± 0.70	1.7 ± 1.7

Table 4.1: Survey of the average material parameters in a sample of 285 fibroblastoid and epithelioid cells.

Finally, our model permits to obtain quantitative information on the value and importance of the isotropic and anisotropic stresses generated by the cells. We combine the shape parameters γ and λ_-/σ with the value of λ_- that we obtain from the magnitudes of the measured forces. In table 4.1 and table 4.2 we report a survey of the parameter values over a sample of 285 cells. Despite the large variability among the cell population, the directed stress α is consistently larger than the isotropic stress σ, reflecting the high anisotropy of the adherent cell types used here.

4.4   Discussion & Conclusion

In conclusion, we have investigated the geometrical and mechanical properties of adherent cells characterized by an anisotropic actin cytoskeleton, by combining experiments on micropillar arrays with simple mechanical modeling. We have predicted and verified that the shape of the cell edge consists of arcs that are described by a unique ellipse, whose major axis is parallel to the orientation of the stress fibers. The model allowed us to obtain quantitative information on the values of the isotropic and anisotropic contractility of cells.

Our work highlights the strong interplay between cell mechanics and geometry. Our model represents a step toward estimating cellular forces from simple imaging data without the need for sophisticated direct force readout. Furthermore, it provides a starting point to study dynamics and explore the role of anisotropy in multicellular environments like tissues [27–30].

4.5   Materials & Methods

4.5.1   Cell culture and fluorescent labeling

Epithelioid GE11 and fibroblastoid GD25 cells [19] expressing either $\alpha 5\beta 1$ or $\alpha v\beta 3$ (GDβ1, GDβ3, GEβ1 and GEβ3) have been cultured as described before [14]. GDβ1, GDβ3, GEβ1 and GEβ3 are approximately equally represented among the 285 cells in the data presented here. Cells have cultured in medium (DMEM; Dulbecco's Modified Eagle's Medium, Invitrogen/Fisher Scientific) supplemented with 10% fetal bovine serum (HyClone, Etten-Leur, The Netherlands), 25 U/ml penicillin and 25 µg/ml streptomycin (Invitrogen/Fisher Scientific cat. # 15070-063). Cells were fixed in 4% formaldehyde and then permeabilized with 0.1% Triton-X and 0.5% BSA in PBS. Tetramethylrhodamine (TRITC)-Phalloidin (Fisher Emergo B.V. cat. # A12380, Thermo Fisher) was subsequently used to stain F-actin [14].

4.5.2 Micropillar arrays

Micropillar arrays were made out of a soft elastomeric material (PDMS) using a negative silicon wafer as a mask as described before [25, 26]. Briefly, the 2 µm diameter micropillars are arranged in a hexagonal pattern with a 4 µm centre-to-centre distance. The micropillars have a height of 6.9 µm, resulting in a stiffness of 16.2 nN/µm. The pillar tops were fluorescently labeled using an Alexa 405-fibronectin conjugate (Alexa Fluor®, Invitrogen/Fisher Scientific, Breda, The Netherlands; Fibronectin cat. #1141, Sigma Aldrich, Zwijndrecht, The Netherlands). Pillar deflections were determined with ∼30 nm precision using a specifically designed Matlab script resulting in a ∼0.5 nN precision in force [26].

4.5.3 Imaging

High-resolution imaging was performed on an in-house constructed spinning disk confocal microscope based on an Axiovert200 microscope body with a Zeiss Plan-Apochromat $100\times$ 1.4NA objective (Zeiss, Sliedrecht, The Netherlands) and a CSU-X1 spinning disk unit (CSU-X1, Yokogawa, Amersfoort, The Netherlands). Imaging was done using an emCCD camera (iXon 897, Andor, Belfast, UK). Alexa405 and TRITC were exited using 405 nm (Crystalaser, Reno, NV) and 561 nm (Cobolt, Stockholm, Sweden) lasers, respectively.

4.5.4 Image analysis

All image analysis and ellipse fitting are performed using Matlab®, except the determination of the stress fiber orientation for which ImageJ with the OrientationJ plugin (`http://bigwww.epfl.ch/demo/orientation/`) was used. The micropillar array allows measuring forces that the cell exerts on the substrate. The forces used in calculations were selected manually when sufficiently large and close to the cell edge. The cell edge is found using a custom script that filters background using a lowpass filter and selects the cell based on a threshold. Then the contour of the cell is divided into parts at the locations of the selected forces. Segments whose straight end-to-end distance is less than 50 pixels (6.9 µm) are discarded, the rest of the segments is used for fitting ellipses.

The orientation of cell edge segments as used in figure 4.1c was calculated by measuring the angle of a line through the two adhesions at either end of the segment. We then defined θ as the angle between this line and the stress fibers.

4.5.5   Ellipse fitting

Ellipses are defined in our experiments with five parameters each: the coordinates of the center of the ellipse, the lengths of the short and long axes, and the angle that the long axis of the ellipse makes with the x-axis of the coordinate system of the image. We use fixed lengths for long and short axes for the N ellipses in the same cell. The optimal ellipse size per cell and positions for each ellipse are found using a $2(N+1)$ parameter fit which minimises the distance between fitted ellipses and cell edge by calculating χ^2. Initial parameters for this fit are obtained from fitting each ellipse separately and averaging the lengths of the axes of the ellipses. Ellipses whose χ^2 is greater than 10 are discarded, which occurs in case of membrane ruffling and other out-of-equilibrium events.

In the global fit, the orientations of the ellipses are fixed to the local orientations of stress fibers. Orientations are measured from the channel with TRITC-Phalloidin (Actin) using the OrientationJ plugin for ImageJ. The average orientation per cell edge segment is calculated over all pixels between 15 and 50 pixels ($2.07\,\mu m$ and $6.9\,\mu m$) away from the cell edge whose coherency is greater than 0.15.

4.5.6   Force analysis

For both the circle and ellipse models, forces on the intersections of circles or ellipses are calculated. For circles, these forces are the vector sum of two forces whose direction is on the tangent to the circle and whose relative magnitude is the radius of the circle. For the ellipse case, the position of the single force on the intersection of two ellipses is first mapped to two forces on a single ellipse. While doing this the short and long axes of the ellipse are rotated and translated such that they coincide with the x and y-axes of the coordinate system. Then two forces $\boldsymbol{F}_1$ and $\boldsymbol{F}_0$ are calculated by combining equation (4.3) and equation (4.4), and defined in such a way that they are pointing clockwise

and counter-clockwise around the ellipse:

$$\frac{\boldsymbol{F}_0}{\lambda_-} = (\beta \sin \phi + \zeta \cos \phi) \, \hat{\boldsymbol{x}} + \left(-\frac{\beta}{\gamma} \cos \phi + \zeta \sin \phi \right) \hat{\boldsymbol{y}}$$

$$\frac{\boldsymbol{F}_1}{\lambda_-} = (\beta \sin \phi - \zeta \cos \phi) \, \hat{\boldsymbol{x}} + \left(-\frac{\beta}{\gamma} \cos \phi - \zeta \sin \phi \right) \hat{\boldsymbol{y}}$$

$$\beta = \frac{d}{2a}$$

$$\zeta = \sqrt{\frac{1 + \tan^2 \phi}{1 + \gamma \tan^2 \phi} - \frac{\beta^2}{\gamma}} \; . \tag{4.5}$$

Here d is the distance between the positions of both forces on the ellipse, a is the length of the long axis of the ellipse and ϕ is the angle that the line through both points makes with the x-axis. After this $\boldsymbol{F}_0$ and $\boldsymbol{F}_1$ are rotated back to the coordinate system of the image and summed to give the force, scaled by λ_-, acting on the cell edge on the location of a particular intersection of two ellipses.

The magnitude of the traction forces is required for the calculation of the minimal line tension λ_- and the isotropic and directed stresses σ and α. We get this from the micropillar array. A measured force usually is the sum of two forces exerted by two different cell edge segments. Therefore, we first decompose the traction force into two forces pointing along tangents to the two cell edge segments adjacent to the position of the force. Then, per cell, we take any combination of two clockwise and counter-clockwise forces and calculate:

$$\lambda_- = \sqrt{\frac{F_{1x}^2 F_{0y}^2 - F_{0x}^2 F_{1y}^2}{F_{0y}^2 - F_{1y}^2}}$$

$$\sigma = \frac{|\boldsymbol{F}_0 - \boldsymbol{F}_1|}{d} \frac{F_{0x} + F_{1x}}{F_{0y} - F_{1y}} \tag{4.6}$$

$$\alpha = \sigma \left(\frac{1}{\gamma} - 1 \right) \; .$$

Here $\boldsymbol{F}_0$ and $\boldsymbol{F}_1$ are defined in the coordinate system where the x and y-axes are the short and long axes of the ellipse. Furthermore, F_{nx} and F_{ny} are the components of $\boldsymbol{F}_n$ in the x and y-directions respectively. To calculate values for these quantities, we average all the different tensions and stresses we get for all possible combinations in all cells, taking the errors on these values into account as weights while averaging.

4.6   Supplementary data

Table 4.1 gives the material parameters γ, λ_-, σ and α for a set of 285 cells. These cells, in fact, come from a pool of two different cell types [14, 19]. The GE11 cells used, exhibit an epithelioid morphology whereas the GD25 cells exhibit a fibroblastoid morphology. Both cell types are deficient of the fibronectin receptor integrin β1. In both cell types, then either α5β1 was reexpressed, or αvβ3 was expressed. These cells are designated GEβ1, GEβ3, GDβ1 and GDβ3. The differing cell and integrin types result in a different cell-substrate coupling leading to different material parameters for each cell and integrin expression type. It is outside the scope of this chapter to examine these differences in detail, therefore initially only the average of each parameter over all 285 cells are given. For completeness, we give the same parameters per cell type in table 4.2. As can be expected [14], cells expressing β1 exert higher traction forces than cells expressing β3, which is reflected in a lower λ_- for the latter.

Cell type	number of cells	γ	λ_- (nN)	σ (nN/μm)	α (nN/μm)
GEβ1	59	0.32 ± 0.14	9.8 ± 6.9	1.4 ± 1.0	2.6 ± 2.2
GEβ3	112	0.31 ± 0.19	5.5 ± 3.4	0.62 ± 0.41	1.3 ± 1.1
GDβ1	56	0.38 ± 0.26	10.6 ± 9.4	0.92 ± 0.78	1.5 ± 1.7
GDβ3	58	0.34 ± 0.25	7.9 ± 6.0	1.0 ± 0.8	2.0 ± 2.2
All	285	0.33 ± 0.20	7.6 ± 5.6	0.87 ± 0.70	1.7 ± 1.7

Table 4.2: Survey of the average material parameters per cell type in a sample of 285 fibroblastoid and epithelioid cells. Shown are the mean and standard deviation. Whereas γ does not vary significantly, there is some variance observed in especially λ_-, which appears larger for cells expressing β-integrin.
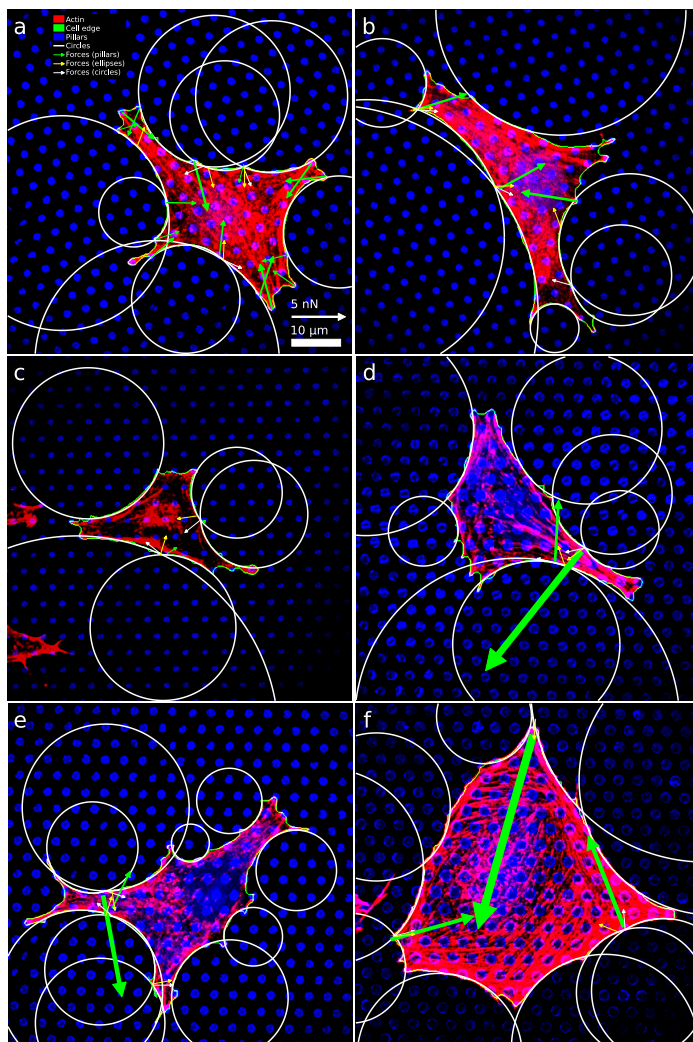
Figure 4.4: **Six examples of cells with circles fitted to the cell edges.**
The actin, cell edge, and micropillar tops are in the red, green and blue channels
respectively. Circles (white) are fitted to the edge of the cells. Orientations
of forces calculated on intersections of either circle from the tension-elasticity
model [11, 18] (white arrows) and the model presented in this chapter (yellow
arrows) are shown as well as the forces measured with the micropillar array
(green arrows). Panels (a) to (c) show epithelioid cells and (d) to (f) show
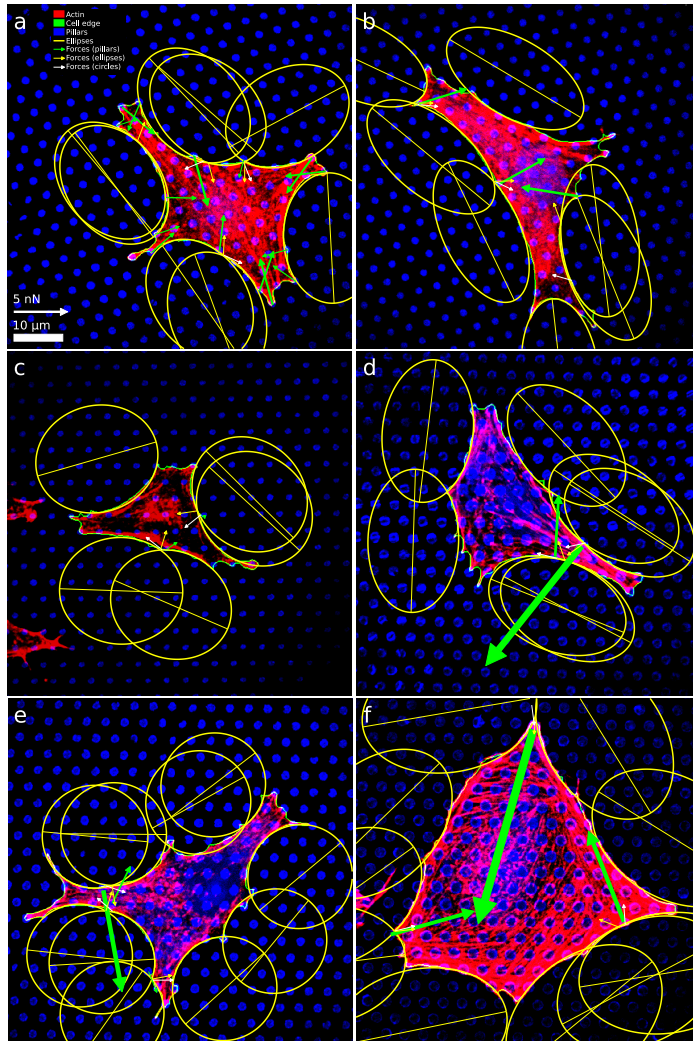fibroblastoid cells.

Figure 4.5: **Six examples of cells (same as in Fig. 4) with ellipses fitted to the cell edges.** The actin, cell edge and micropillar tops are in the red, green and blue channels respectively. Ellipses (yellow, including the long axis) are fitted to the edge of the cells. Orientations of forces calculated on intersections of either circles form the tension-elasticity model [11, 18] (white arrows) and the model presented in this chapter (yellow arrows) are shown as wel as the forces measured with the micropillar array (green arrows). Panels (a) to (c) show epithelioid cells and (d) to (f) show fibroblastoid cells. Fit values for the ellipses in panels (a) to (f) respectively: γ: 0.52; 0.25; 0.75; 0.40; 0.95; 0.46, λ_-/σ (μm): 13.4; 15.7; 12.6; 14.7; 10.8; 18.0.

References

[1] B. Geiger, J. P. Spatz, and A. D. Bershadsky. "Environmental sensing through focal adhesions". In: *Nat. Rev. Mol. Cell Biol.* 10.1 (2009), pp. 21–33. DOI: 10.1038/nrm2593.

[2] D. E. Discher, P. Janmey, and Y. L. L. Wang. "Tissue cells feel and respond to the stiffness of their substrate". In: *Science* 310.5751 (2005), pp. 1139–1143. DOI: 10.1126/science.1116995.

[3] F. Jülicher et al. "Active behavior of the Cytoskeleton". In: *Phys. Rep.* 449.1-3 (2007), pp. 3–28. DOI: 10.1016/j.physrep.2007.02.018.

[4] B. D. Hoffman, C. Grashoff, and M. a. Schwartz. "Dynamic molecular processes mediate cellular mechanotransduction". In: *Nature* 475.7356 (2011), pp. 316–323. DOI: 10.1038/nature10316.

[5] M. G. Mendez and P. A. Janmey. "Transcription factor regulation by mechanical stress". In: *Int. J. Biochem. Cell Biol.* 44.5 (2012), pp. 728–732. DOI: 10.1016/j.biocel.2012.02.003.

[6] A. J. Engler et al. "Matrix elasticity directs stem cell lineage specification". In: *Cell* 126.4 (2006), pp. 677–89. DOI: 10.1016/j.cell.2006.06.044.

[7] B. Trappmann et al. "Extracellular-matrix tethering regulates stem-cell fate". In: *Nat. Mater.* 11.7 (2012), pp. 642–9. DOI: 10.1038/nmat3339.

[8] Y. Sawada et al. "Force sensing by mechanical extension of the Src family kinase substrate p130Cas". In: *Cell* 127.5 (2006), pp. 1015–1026. DOI: 10.1016/j.cell.2006.09.044.

[9] C. M. Lo et al. "Cell movement is guided by the rigidity of the substrate". In: *Biophys. J.* 79.1 (2000), pp. 144–152. DOI: 10.1016/S0006-3495(00)76279-5.

[10] R. D. Sochol et al. "Unidirectional mechanical cellular stimuli via micropost array gradients". In: *Soft Matter* 7.10 (2011), pp. 4606–4609. DOI: 10.1039/c1sm05163f.

[11] I. B. Bischofs, S. S. Schmidt, and U. S. Schwarz. "Effect of adhesion geometry and rigidity on cellular force distributions". In: *Phys. Rev. Lett.* 103.4 (2009), p. 048101. DOI: 10.1103/PhysRevLett.103.048101.

[12] M. Ghibaudo et al. "Substrate topography induces a crossover from 2D to 3D behavior in fibroblast migration". In: *Biophys. J.* 97.1 (2009), pp. 357–368. DOI: 10.1016/j.bpj.2009.04.024.

[13] D. A. Fletcher and R. D. Mullins. "Cell mechanics and the cytoskeleton".
      In: *Nature* 463.7280 (2010), pp. 485–92. DOI: 10.1038/nature08908.

[14] H. E. Balcioglu et al. "The integrin expression profile modulates orienta-
      tion and dynamics of force transmission at cell-matrix adhesions". In: *J.
      Cell Sci.* 128.7 (2015), pp. 1316–1326. DOI: 10.1242/jcs.156950.

[15] U. S. Schwarz and S. A. Safran. "Physics of adherent cells". In: *Rev. Mod.
      Phys.* 85.3 (2013), pp. 1327–1381. DOI: 10.1103/RevModPhys.85.1327.

[16] L. Giomi. "Softly constrained films". In: *Soft Matter* 9.34 (2013), pp. 8121–
      8139. DOI: 10.1039/c3sm50484k.

[17] R. Bar-Ziv et al. "Pearling in cells: A clue to understanding cell shape".
      In: *Proc. Natl. Acad. Sci.* 96.18 (1999), pp. 10140–10145. DOI: 10.1073/
      pnas.96.18.10140.

[18] I. B. Bischofs et al. "Filamentous network mechanics and active con-
      tractility determine cell and tissue shape". In: *Biophys. J.* 95.7 (2008),
      pp. 3488–3496. DOI: 10.1529/biophysj.108.134296.

[19] E. H. J. Danen et al. "The fibronectin-binding integrins $\alpha5\beta1$ and $\alpha v\beta3$
      differentially modulate RhoA–GTP loading, organization of cell matrix
      adhesions, and fibronectin fibrillogenesis". In: *J. Cell Biol.* 159.6 (2002),
      pp. 1071–1086. DOI: 10.1083/jcb.200205014.

[20] S. Pellegrin and H. Mellor. "Actin stress fibres". In: *J. Cell Sci.* 120.20
      (2007), pp. 3491–3499. DOI: 10.1242/jcs.018473.

[21] K. Burridge and E. S. Wittchen. "The tension mounts: Stress fibers
      as force-generating mechanotransducers". In: *J. Cell Biol.* 200.1 (2013),
      pp. 9–19. DOI: 10.1083/jcb.201210090.

[22] T. J. Pedley and J. O. Kessler. "Hydrodynamic phenomena in suspensions
      of swimming microorganisms". In: *Annu. Rev. Fluid Mech.* 24.1 (1992),
      pp. 313–358. DOI: 10.1146/annurev.fl.24.010192.001525.

[23] R. Aditi Simha and S. Ramaswamy. "Hydrodynamic fluctuations and
      instabilities in ordered suspensions of self-propelled particles". In: *Phys.
      Rev. Lett.* 89.5 (2002), p. 058101. DOI: 10.1103/PhysRevLett.89.
      058101.

[24] J. L. Tan et al. "Cells lying on a bed of microneedles: An approach to
      isolate mechanical force". In: *Proc. Natl. Acad. Sci. U. S. A.* 100.4 (2003),
      pp. 1484–1489. DOI: 10.1073/pnas.0235407100.

[25] L. Trichet et al. "Evidence of a large-scale mechanosensing mechanism
      for cellular adaptation to substrate stiffness". In: *Proc. Natl. Acad. Sci.
      U. S. A.* 109.18 (2012), pp. 6933–6938. DOI: 10.1073/pnas.1117810109.

[26] H. Van Hoorn et al. "The nanoscale architecture of force-bearing focal adhesions". In: *Nano Lett.* 14.8 (2014), pp. 4257–4262. DOI: `10.1021/nl5008773`.

[27] M. Eastwood et al. "Effect of precise mechanical loading on fibroblast populated collagen lattices: Morphological changes". In: *Cell Motil. Cytoskeleton* 40.1 (1998), pp. 13–21. DOI: `10.1002/(SICI)1097-0169(1998)40:1<13::AID-CM2>3.0.CO;2-G`.

[28] D. W. van der Schaft et al. "Mechanoregulation of vascularization in aligned tissue-engineered muscle: A role for vascular endothelial growth factor". In: *Tissue Eng. Part A* 17.21-22 (2011), pp. 2857–2865. DOI: `10.1089/ten.tea.2011.0214`.

[29] R. F. M. van Oers et al. "Mechanical cell-matrix feedback explains pairwise and collective endothelial cell behavior in vitro". In: *PLoS Comput. Biol.* 10.8 (2014), e1003774. DOI: `10.1371/journal.pcbi.1003774`.

[30] D. S. Vijayraghavan and L. A. Davidson. "Mechanics of neurulation: From classical to current perspectives on the physical mechanics that shape, fold, and form the neural tube". In: *Birth Defects Res.* 109.2 (2017), pp. 153–168. DOI: `10.1002/bdra.23557`.